submitted manuscript has been authored
contractor of the U. S. Government
contract No. W-31-109-ENG-38.
rdingly, the U. S. Government retains a
xclusive, royalty-free license to publish
reproduce the published form of this
ribution, or allow others to do so, for
. Government purposes.

ANL-HEP-CP-93-06

Fermilab Library
0 1160 0022713 4

ANL-HEP-CP-93-06
For the Proceedings of the
10th International Symposium on
High Energy Spin Physics
Nagoya, Japan
9-14 November 1992

RECENT EXPERIMENTS ON SPIN PHYSICS IN HIGH ENERGY HADRON INTERACTIONS*

Akihiko YOKOSAWA
High Energy Physics Division
Argonne National Laboratory, Argonne, Illinois 60439 USA

ABSTRACT

We review recent spin-physics experiments in high-energy hadron interactions, significant physics accomplished, and future prospects.

FERMILAB
MAR 0 8 1993
LIBRARY

1. Experiments with Polarized Beams at Fermilab

1.1 Polarized Beam (protons and antiprotons) Facility

An extracted beam from the Tevatron is delivered through the MP primary-beam line to the Meson Detector Building where a 0.73-interaction-length Be target is utilized to produce Λ and $\bar{\Lambda}$ at $\theta_{c.m.} \approx 0°$. Protons and antiprotons from the Λ and $\bar{\Lambda}$ decays respectively are brought to a final target position in the MP hall through the MP secondary beam (200 GeV/c) line.

Polarized protons from the virtual sources are focused in the tagging section, where both the momentum and polarization are selected.[1] The typical beam flux ($\Delta p/p = \pm 5\%$) for 3×10^{12} incident protons per 20-sec spill at 200 GeV/c were: (P_{av} is average polarization)

	Tagged Beam (P_{av} = 45%)	Total Particles	Background π's
Protons	1.0×10^7	2.0×10^7	2.0×10^6
Antiprotons	5.0×10^5	1.0×10^6	5.0×10^6

1.1.1 Primakoff-Effect Measurement

The asymmetry of the nuclear coherent Coulomb $\pi°$ production process ("Primakoff Process"), was measured[2] for the first time with the use of the 200-GeV/c polarized-proton beam. The apparatus consisted of a lead-glass calorimeter for $\pi°$ detection and a magnetic spectrometer for

the scattered protons. A large asymmetry in the region of $|t'| < 0.001$ $(GeV/c)^2$ and $1.36 < M(\pi^\circ p) < 1.52$ GeV/c^2 was observed for the reaction $p + Pb \rightarrow p + \pi^\circ + Pb$, where the Coulomb process is predominant.

1.1.2 Coulomb-Nuclear Interference (CNI) Measurement

Several authors since Schwinger[3] have indicated nonzero polarization in the Coulomb-nuclear interference region in nucleon-nucleon scattering. This polarimeter is to measure the interference term of the nonflip amplitude and the electromagnetic spin-flip amplitude. The proton polarization arising from the interference is $P \approx 5\%$ at $|t| = 2 \cdot 10^{-3}$ $(GeV/c)^2$ and is energy independent.[4]

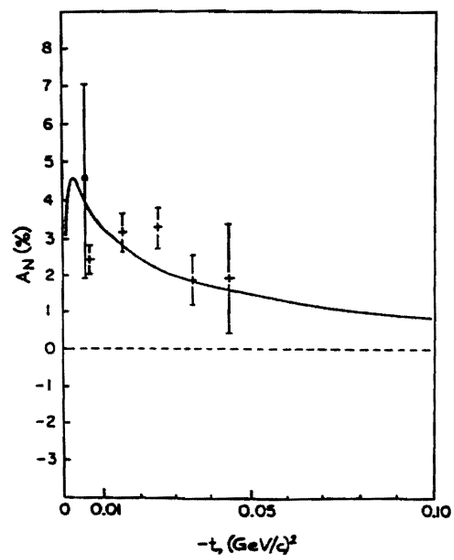

Figure 1. pp analyzing power in the Coulomb-nuclear region.

The analyzing power, A_N, of proton-proton, proton-hydrocarbon, and antiproton-hydrocarbon scattering in the Coulomb-nuclear region was earlier measured using the 200-GeV/c polarized beams.[5] These results are consistent with predictions[6-8] based on Coulomb-nuclear interference.

Recently a new CNI target consisting of trans-stilbene crystals (diphenyl-ethylene, $C_{14}H_{12}$) was used.[9] Large background was reduced at small $|t|$ region by using this material that possesses pulse-shaped discrimination characteristics. Preliminary results on the pp analyzing power are shown in Fig. 1 together with the calculated values.

1.2 Hadron Production with 200-GeV/c Polarized Proton and Antiproton Beams

1.2.1 Single-Spin Asymmetry in $p^\uparrow p \rightarrow (\pi^\circ, \eta)$ and $\bar{p}^\uparrow p \rightarrow \pi^\circ X$ at high $p_\perp$

Asymmetry measurements, $A_N = (1/P_B)(N^\uparrow - N^\downarrow)/(N^\uparrow + N^\downarrow)$, were carried out at 200 GeV/c in π° and η production. Photons from the decay of π°s produced in the target are detected in the "Central Electromagnetic Calorimeters", shown in Fig. 2, located at 10 m from the target. Each calorimeter is comprised of 504 lead-glass counters in an array of 21 columns by 24 rows. The dimensions of each lead-glass block are 3.81 cm × 3.81 cm × 18 radiation lengths.

Data of the $p^\uparrow p$ reaction[10] show that the asymmetry values (A_N) at $x_F \approx 0$ are approximately zero (or small negative) up to $p_\perp = 3.5$ GeV/c and then begin to rise to ~ + 40% in the region of $p_\perp = 4$ to 5 GeV/c as shown in Fig. 3.

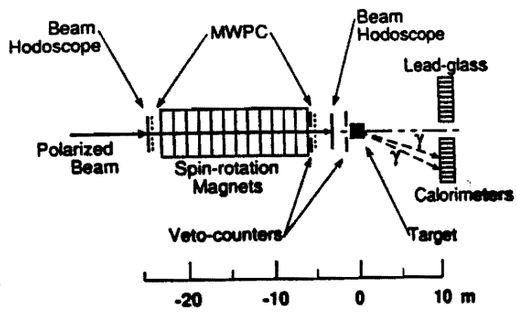

Figure 2. Layout of the experimental apparatus.

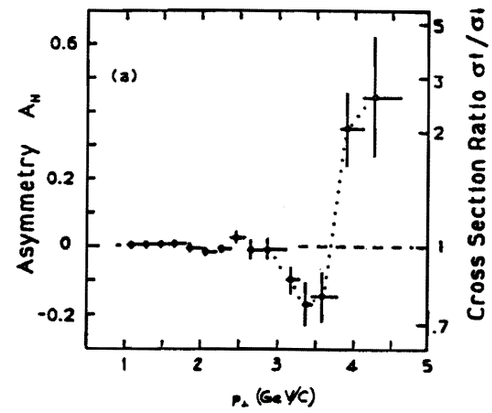

Figure 3. $p_\perp$ dependence of A_N at $x_F = 0$.

At lower energies as seen in the BNL[11] ($p^\uparrow p \to \pi^+X$), CERN[12] ($pp^\uparrow \to \pi^\circ X$), Serpukhov[13] ($\pi p^\uparrow \to \pi^\circ X$) data, this rapid rise from zero to large positive values, was also observed although none of the data exceeded $p_\perp = 3$ GeV/c. A positive sign of A_N mentioned above corresponds to a larger production cross section to beam-left (beam-right) when the beam (target) proton is vertically-upward. Note that for the usual sign convention, $A_N (p^\uparrow h \to hX) = -A_N (hp^\uparrow \to hX)$ at $x \approx 0$ where h represents hadron. A new finding is that all the A_N data of π° or π^+ production at $x_F \approx 0$ show the large positive asymmetries begin at $x_\perp = 0.4$ in the region $\sqrt{s} = 5$ to 20 GeV. This is strong indication that we are indeed observing asymmetries caused by hard scattering.

Single-spin asymmetry in $\bar{p}^\uparrow p \to \pi^\circ X$ shows a similar $p_\perp$ dependence as the $p^\uparrow p$ case. However, data are limited only up to $p_\perp = 3.5$ GeV/c . We have also observed a similar $p_\perp$ dependence in $p^\uparrow p \to \eta X$.

Asymmetry measurements (A_N) in $p^\uparrow p \to \pi^\circ X$ and $\bar{p}^\uparrow p \to \pi^\circ X$ on the x_F dependence covering $p_\perp$ up to 2 GeV/c were carried out.[14] A_N values in the $p^\uparrow p$ reaction are consistent with zero up to $x_F = 0.3$ to 0.4, and then linearly increase to + 20% near $x_F = 1.0$ as shown in Fig. 4. Also they are consistent with earlier data[15] taken at $\langle x_F \rangle = 0.52$.

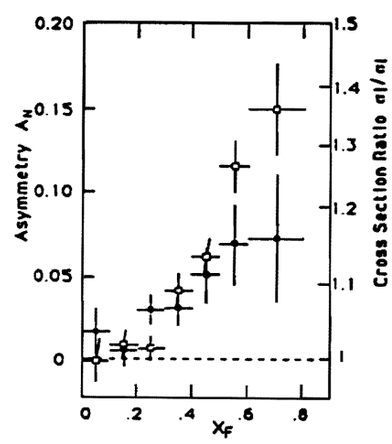

Figure 4. x_F dependence of A_N at $p_\perp = 0.5$ to 2.0 GeV/c the reaction $p^\uparrow p \to \pi^\circ X$ (open squares) and $\bar{p}p \to$(closed circles).

1.2.2 x_F Dependence of Single-Spin Asymmetry in $p^\uparrow p \to \pi^\circ X$ and $\bar{p}^\uparrow p \to \pi^\circ X$

Single spin asymmetry in $\bar{p}^{\uparrow}p$ reaction shows a similar x_F dependence as $p^{\uparrow}p$ case. By knowing the quark content of $\pi^{\circ} = (u\bar{u} - d\bar{d})/\sqrt{2}$, both the polarized u and $\bar{u}$ quark in the polarized proton and antiproton beam respectively seems to be the carrier of the spin information. We can also interpret these results using a dynamical mechanism[16] describing the spin effect in the inclusive hadron production in the fragmentation region. In this mechanism, asymmetries in $pp \rightarrow \pi^{\circ}X$ and $\bar{p}p \rightarrow \pi^{\circ}X$ are related to the πp backward scattering as i) $\pi^{\circ}p \rightarrow p\pi^{\circ}$ and ii) $\pi^{\circ}\bar{p} \rightarrow \bar{p}\pi^{\circ}$, respectively. By applying the CPT conservation, the antiprocess of the i) is the process ii). Thus, similar x_F dependence in asymmetries by protons and antiprotons can be explained.

It is interesting to notice that our data resembled x_F dependence in $pp \rightarrow \Lambda^{\uparrow}X$ where polarized s quarks were considered[17] to be responsible for high polarization.

1.2.3 x_F Dependence of Single-Spin Asymmetry in $p^{\uparrow}p \rightarrow \pi^{\pm}X$ and $\bar{p}^{\uparrow}p \rightarrow \pi^{\pm}X$

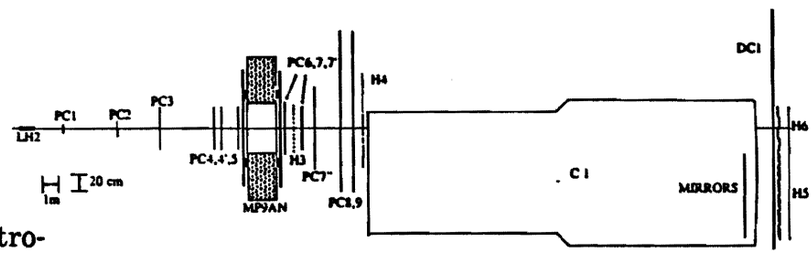

Figure 5. Top view of the E-704 forward spectrometer layout.

Single-spin asymmetries were measured in $\pi^{\pm}$ production at 200 GeV/c.[18] Pion production from the target was measured via a large forward spectrometer which is shown in Fig. 5. The asymmetry values (A_N) in the $p^{\uparrow}p$ reaction are shown in Fig. 6 as a function of x_F for the π^+ and π^- data over a $p_{\perp}$ range of 0.2 - 2.0 GeV/c. The data exhibit a striking form in which the magnitude of A_N increases for both π^+ and π^- particles with x_F, but the sign of A_N is negative for the π^- data. Further study of these data shows a threshold effect in which A_N increases dramatically above $p_{\perp} = 0.7$ GeV/c.

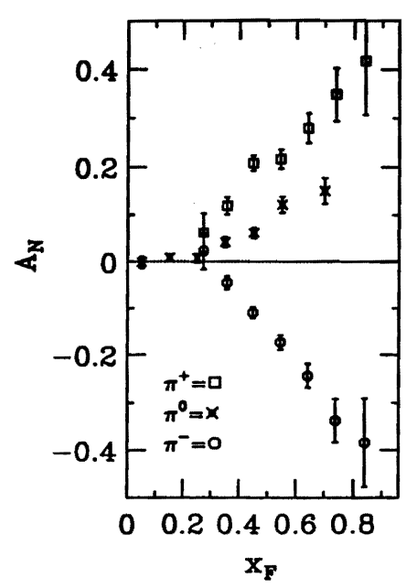

Figure 6 A_N for π^+ (squares) and π^- (circles) production in the $p^{\uparrow}p$ reaction versus x_F integrated over $p_{\perp}$. For comparison, π^0 data (crosses) are also plotted.

From this mirror-symmetry effect in π^+ and π^-, one may speculate $A_N = 0$ for π° production. By applying isospin relations for single-particle distributions,[19] $\sigma^+ A_N^+ + \sigma^- A_N^- = 2\,\sigma^\circ A_N^\circ$, where σ^+ and A_N^+ are for the cross section and analyzing power in $p^\uparrow p \to \pi^+ X$ respectively, σ^- and A_N^- in $p^\uparrow p \to \pi^- X$, and σ° and A_N° in $p^\uparrow p \to \pi^\circ X$, we can conclude the following: Experimental data show $\sigma^+ > \sigma^-$ and $A_N^+ \approx -A_N^-$, therefore we expect $A_N^\circ > 0$ as shown in Fig. 4.

The A_N values in the $\bar{p}^\uparrow p$ reaction[20] are shown in Fig. 7 for the π^+ and π^- data. We observe a similar behavior on A_N magnitude with respect to x_F but the sign of A_N is positive for the π^- data and negative for the π^+ data. The results can be explained by using the model[16] which relate $pp \to \pi^\pm X$ scattering to the πp backward scattering. The antiprocesses of $\pi^+ p \to p\pi^+$ and $\pi^- p \to p\pi^-$ are $\pi^- \bar{p} \to \bar{p}\pi^-$ and $\pi^+ \bar{p} \to \bar{p}\pi^+$ respectively. Thus we have opposite signs for $p^\uparrow$ and $\bar{p}^\uparrow$ beams.

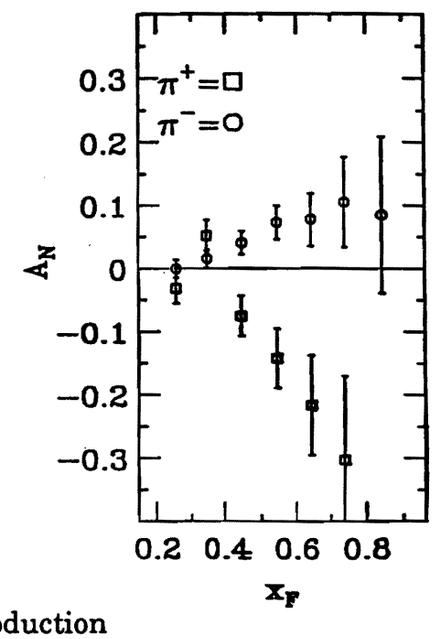

Figure 7. A_N for π^+ (squares) and π^- (circles) in the $\bar{p}^\uparrow p$ reaction.

1.2.4 Double-Spin Asymmetry in π° Production

We report on a first measurement of the two-spin parameter A_{LL} for inclusive π° production by 200-GeV longitudinally-polarized protons and antiprotons on a longitudinally-polarized proton target.[21] The hadron asymmetry A_{LL} is defined as the relative difference between the cross sections for beam and target hadrons of equal or opposite helicities,

$$A_{LL} = (\sigma^{\rightleftarrows} - \sigma^{\rightrightarrows}) / (\sigma^{\rightleftarrows} + \sigma^{\rightrightarrows})$$
$$= P_B^{-1} \bullet \langle P_T \rangle^{-1} \bullet \left(N^{\rightleftarrows} - N^{\rightrightarrows}\right) / \left(N^{\rightleftarrows} + N^{\rightrightarrows}\right),$$

where $\sigma(s, x_F, p_t)$ are the invariant cross sections in antiparallel ($\rightleftarrows$) and parallel ($\rightrightarrows$) spin states of the beam and target particles. Since the incident hadrons have opposite momenta in the c.m. of the interaction, the helicities are equal when the spin directions are not parallel.

The results[22] for A_{LL} measured for incident protons and antiprotons as a function of $p_\perp$ show that each value for A_{LL} in the $p_\perp$ interval covered by these measurements is consistent with zero, within the statistical errors.

1.3 One-Spin and Two-Spin Measurements in Λ Production

To explain spin effects in hyperon production, many have proposed a wide range of mechanisms but none of them completely explains all the data. At 200 GeV/c, three parameters were measured for further understanding of Λ asymmetry effects; they are the polarization P, the analyzing power A, and the depolarization D.

1.4 Difference in Total Cross Sections, $\Delta\sigma_L$

The difference between total cross sections with spins antiparallel and with spins parallel longitudinally was measured at 200 GeV/c.

$$\Delta\sigma_L = \left[\sigma^{Tot}\left(\rightleftarrows\right) - \sigma^{Tot}\left(\rightrightarrows\right)\right].$$

Only preliminary data are available currently.

2. Brief Review of Proton-Proton Elastic Scattering at High $p_\perp$

Earlier studies on proton-proton (pp) elastic scattering are summarized, Ref. 23. With polarized-proton beams at BNL, the analyzing power, A_N, and spin-spin correlation parameter, A_{NN}, were measured[24] up to incident proton-laboratory momentum of 24 GeV/c and $p_\perp^2$ up to 7.1 $(GeV/c)^2$. As shown in Fig. 8, values of A_N increase as $p_\perp^2$. A similar trend is observed in the hadron production as described earlier.

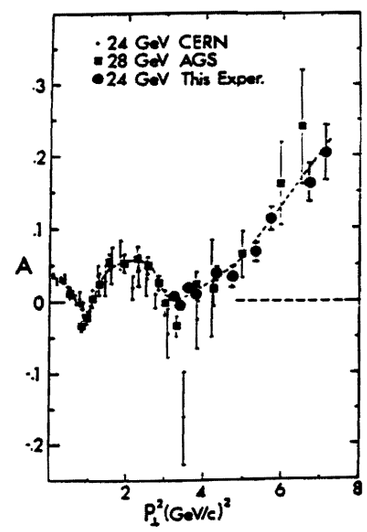

Figure 8. A_N in pp elastic scattering.

3. Brief Report on Experiments at IHEP, Serpukhov

The single-spin asymmetry A_N in the inclusive reaction $\pi^- d^\uparrow \rightarrow \pi^\circ X$ in the beam fragmentation region at 40 GeV/c was measured. A frozen-spin ($C_3D_8O_2$) polarized target was used. The p_T dependence of the A_N was observed as similar to the one in case of hyperon polarization over the interval $0.7 < x_F < 0.9$.

4. Study of the Spin-Dependent Parton Distribution with Polarized Protons[25]

These studies can be made at Fermilab polarized-beam facility, planned polarized beams at UNK, and proposed polarized collider at RHIC. In fact, the major motivation to construct the Fermilab

polarized-beam facility was to obtain the gluon-spin information by measuring the asymmetry parameter A_{LL} for χ_2 and J/ψ production (proposal 675) and was many years before the "spin crisis".

4.1 Measurements of Parton Helicity Distribution in a Polarized Proton

4.1.1 Gluon Helicity Distribution

i) Direct-γ Production

Direct photons are produced through the $q\bar{q}$ annihilation subprocess and the q-g Compton subprocess, $qg \rightarrow \gamma q$. The Compton process is the dominant one in pp interactions. Then,

$$A_{LL} = [\Delta u(x_1)/u(x_1)] \bullet [\Delta G(x_2)/G(x_2)] \bullet \hat{a}_{LL}(qg \rightarrow \gamma q).$$

ii) Jet Production

Several QCD subprocesses contribute to the cross section for jet production:

a) gluon-gluon scattering at low $p_\perp$,
b) gluon-quark scattering at medium $p_\perp$ (above ~ 20 GeV/c), and
c) quark-quark elastic scattering at high $p_\perp$.

4.1.2 Sea-Quark Helicity Distribution - Drell-Yan Process

The Drell-Yan process appears to be one of the best ways to determine the polarization of sea quarks. The $q\bar{q}$ annihilation into a vector boson gives a large asymmetry at the partonic level, and selects sea antiquarks along with valence quarks.

The asymmetry A_{LL} for Drell-Yan in pp collisions is related to the sea-quark helicity distribution.

4.2 Parity-Violating Asymmetry in W and Z Production

W and Z production with polarized protons is a totally unexplored area. The predictions for asymmetries, in particular, for the parity nonconservation ones, are expected to be large. The observable A_L^{pv} contains spin information for sea quarks.

4.3 Measurements of Quark Transversity Distribution in Polarized Protons

From deep inelastic scattering, one can measure $f_1(x)$ related to the longitudinal momentum distribution of quarks in the nucleon and $g_1(x)$ related to the helicity distribution of a polarized nucleon. There exists a third fundamental function, $h_1(x)$, which is a leading-twist (twist-2) distribution function like $f_1(x)$ and $g_1(x)$. This can be determined by measuring the transverse spin asymmetry A_{NN} in Drell-Yan processes.

4.4 One-Spin Measurement to Determine Spin-Dependent Quark-Gluon Correlation Functions

Single transverse spin asymmetries in hard processes are expected to vanish in pQCD. The asymmetries vanish at the leading-twist (2) level, however, this is no longer true at twist-3. The twist-3 parton distribution involves the correlation between quark and gluon field strength.[26]

5. RHIC Polarized Collider and the STAR Detector

The RHIC polarized collider and associated experiments will be covered by several colleagues. RHIC spin proposal, R5, contains experiments using detectors STAR and PHENIX. Here, I would like to describe how accurately measurements can be made within the acceptance of the STAR detector (see Fig. 9).

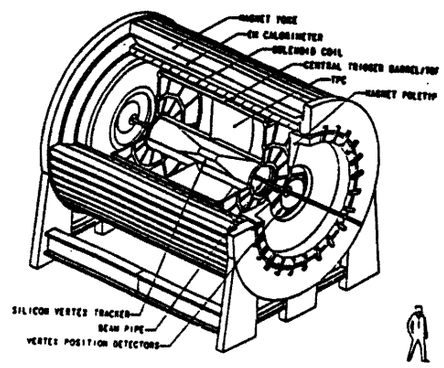

Figure 9. Perspective view of the STAR experimental configuration.

There are several areas of proton-proton spin physics that can be best done with a combination of RHIC and STAR.

We present the estimates of the acceptances of STAR and expected event rates for various reactions discussed earlier.

The integrated luminosities used are:

$$\int \mathcal{L}dt = 3.2 \cdot 10^{38}\ \mathrm{cm}^{-2} \text{ at } 200\ \mathrm{GeV} = 320\ \mathrm{pb}^{-1},$$

which means 100 days of running ($4 \cdot 10^6$ sec, 50% eff.).

5.1 Measurements with Barrel EM Calorimeter and Shower Maximum Detector

a) Direct-γ Production

At $\sqrt{s}$ = 200 GeV,

$$\delta A_{LL} \sim \pm (1/P^2)\,(0.003\sqrt{3.2 \times 10^{38}\ \mathrm{cm}^{-2}/\int \mathcal{L}dt})\,.$$

b) Direct-γ + Jet

"γ + Jet" events with $-0.3 < \eta_{jet} < 0.3$ and $-1.0 < \eta_\gamma < 1.0$ determine the kinematics of the primary quark-gluon scattering.

For the p_T acceptance of 10 to 20 GeV, x_1 and x_2 vary from 0.1 to 0.2 at $\sqrt{s}$ = 200 GeV. For the cross section in the p_T interval 15-20 GeV/c equal to 28 pb, the estimated uncertainty in A_{LL} is:

$$\delta A_{LL} \sim \pm (1/P^2)\,(0.017\sqrt{3.2 \times 10^{38}\ \mathrm{cm}^{-2}/\int \mathcal{L}dt})\,.$$

c) A_L^{PV} in W and Z Production

The STAR detector with electromagnetic calorimeters is especially suitable for experiments with the W and Z due to its large acceptance for electrons produced by high mass particle decays. The events rates at $\sqrt{s}$ = 500 GeV are:

Boson	STAR (Barrel)
$W^+ + W^-$	83,000
W^+	61,000
W^-	22,000
Z°	3,840

5.2 Measurements with Endcaps

An important upgrade for the photon detection would be a pair of EM endcap calorimeters to be placed inside the iron pole piece. They would cover $|\eta| \leq 2.0$. We show accuracy for some of the reactions discussed earlier.

a) Detecting with Direct-γ and the "Away-Side" Jet (200 GeV)

δA_{LL}, Uncertainty in Asymmetry

	max (x_1, x_2)			
min (x_1, x_2)	≤ 0.2	0.2 - 0.3	0.3 - 0.4	> 0.4
0.00 - 0.05		0.012	0.009	0.007
0.05-0.10	0.006	0.006	0.010	0.012
0.10-0.15	0.007	0.010	0.020	0.030
0.15-0.20	0.021	0.019	0.038	0.060
> 0.20		0.035	0.049	0.073

b) Sea-Quark Helicity Distribution (200 GeV)

M_{ee}, GeV/c^2	5-9	9-12	12-15	15-20
	28,000	20,000	8,400	5,400

* Work supported by the U.S. Department of Energy, Division of High Energy Physics, Contract W-31-109-ENG-38.

6. References

1) D. Grosnick et al., 1990, *Nucl. Instrum. and Meth.* **A290**, 269.
2) D. C. Carey et al., 1990, *Phys. Rev. Lett.* **64**, 357.
3) J. Schwinger, 1948, *Phys. Rev.* **73**, 407.
4) For instance, C. Bourrely and J. Soffer, 1977, *Nuovo Cimento Lett.* **19**, 569.
5) N. Akchurin et al., 1989, *Phys. Lett.* **B229**, 299.
6) B. Z. Kopeliovich and L. I. Lapidus, 1974, Yad. Fig. **19**, 218; 1974, *Sov. J. Nucl. Phys.* **19**, 114.
7) N. H. Buttimore, E. Gotsman , and Am. E. Leader, 1978, *Phys. Rev.* **D18**, 694.
8) N. H. Buttimore, 1985, *Proc. 6th Int. Symp. on High Energy Spin Physics,* Marseille, Ed. J. Soffer, Journal de Physique, **46**, C2, 643.
9) N. Akchurin et al., to be published.
10) D. L. Adams et al., 1992, *Phys. Lett.*, **B276**, 531.
11) S. Sanoff et al., 1990, *Phys. Rev. Lett.* **64**, 995.
12) J. Antille et al., 1980, *Phys. Lett.* **B94**, 523.
13) V. D. Apokin et al., 1990, *Phys. Lett.* **B243**, 461.
14) D. L. Adams et al., 1991, *Phys. Lett.* **B261**, 201; 1992, *Zeit Phys.* **C56**, 181.
15) B. E. Bonner et al., 1988, *Phys. Rev. Lett.* **61**, 1918.
16) J. Soffer and N. A. Tornquist, 1992, *Phys. Rev. Lett.* **68**, 907.
17) T. deGrand and H. I. Miettinen, 1981, *Phys. Rev.* **D24**, 2419; 1985, *Phys. Rev.* **D31** (E) 661.
18) D. L. Adams et al., 1991, *Phys. Lett.* **B264**, 462.
19) J. Soffer and D. Wray, Wis-72/31-ph, unpublished.
20) E-704 preliminary data.
21) P. Chaumette et al., 1990, *Proc. 9th Int. Symp. on High Energy Spin Phys.*, Bonn, Germany, p. 237.
22) D. L. Adams et al., 1991, *Phys. Lett.* **B261**, 197.
23) A. Yokosawa, 1990, *International Journal of Modern Physics A,* Vol. 5, No. 16, p. 3089, and references therein.
24) D. G. Crabb et al., 1990, *Phys. Rev. Lett.* **65**, 3241.
25) This is a brief description of Physics Issues for the RHIC polarized collider. For references, see proposal R5 dated August 14, 1992.
26) J. Qiu and G. Sterman, 1991, *Phys. Rev. Lett.* **67**, 2264.